Applied Mathematical Modelling 143 (2025) 116035

Contents lists available at ScienceDirect

Applied Mathematical Modelling

journal homepage: www.elsevier.com/locate/apm

A meshfree approach for the rennet-induced coagulation equation: Spline based multistage Bernstein collocation method and its convergence analysis

Nikhil Sriwastav [a,b,e], Ashok Das [a,b,c], Orest Shardt [a,b], Jitendra Kumar [d], Mehakpreet Singh [a,e,*]

[a] Dairy Processing Technology Centre, University of Limerick, Limerick, V94 T9PX, Ireland
[b] Department of Chemical Sciences, Bernal Institute, University of Limerick, Limerick, V94 T9PX, Ireland
[c] Department of Mathematics, Indian Institute of Technology (ISM), Dhanbad, India
[d] Department of Mathematics, Indian Institute of Technology, Ropar 14001, India
[e] Mathematics Applications Consortium for Science and Industry (MACSI), Department of Mathematics & Statistics, University of Limerick, V94T9PX Limerick, Ireland

ARTICLE INFO

Keywords:
Rennet coagulation
Cheese manufacturing
Nonlinear integro-partial differential equations
Multi stage Bernstein polynomials
Finite volume scheme

ABSTRACT

The initial phases of milk coagulation for cheese manufacturing can be tracked by an integro-differential equation known as a population balance equation. In this article, a new analytical approach using multistage Bernstein polynomials is presented to solve a rennet-induced coagulation equation for the first time. The existence of the solution and convergence analysis of the proposed approach are discussed in detail to support the mathematical formulation. Our main interest is in computing the integral moments, such as the number and total volume/mass of casein micelles over time. These moments are evaluated by approximating them with the linear combinations of Bernstein polynomials that involve unknown coefficients. Furthermore, the unknown coefficients are determined by selecting an appropriate number of collocation points, based on the considered time span of the process. To test the accuracy and efficiency of the new approach, the new analytical solutions for the integral moments are obtained for constant, sum and product coagulation kernels and results are verified by comparing with the existing finite volume scheme and Picard's method.

Contents

1. Introduction . . . 2
   1.1. Literature review and motivation . . . 3
2. Existence theorem . . . 4
3. Basics of multistage Bernstein polynomials . . . 6
   3.1. Bernstein polynomials . . . 6

* Corresponding author at: Mathematics Applications Consortium for Science and Industry (MACSI), Department of Mathematics & Statistics, University of Limerick, V94T9PX Limerick, Ireland.
E-mail addresses: nikhilsrivastava416908@gmail.com (N. Sriwastav), ashokdas@iitism.ac.in (A. Das), Orest.Shardt@ul.ie (O. Shardt), jkumar@iitrpr.ac.in (J. Kumar), Mehakpreet.Singh@ul.ie (M. Singh).

https://doi.org/10.1016/j.apm.2025.116035
Received 21 October 2024; Received in revised form 17 February 2025; Accepted 19 February 2025

Available online 21 February 2025

3.2. Generalized Bernstein polynomials . . . 6
3.3. Bernstein function approximation . . . 6
3.4. Spline based multi-stage Bernstein collocation method . . . 6
4. Convergence analysis . . . 7
5. Numerical testing and discussion . . . 8
5.1. Coagulation without proteolysis process . . . 9
5.1.1. Size-independent constant kernel . . . 9
5.1.2. Size-dependent sum kernel . . . 9
5.2. Coagulation with proteolysis process . . . 10
5.2.1. Constant kernel . . . 10
5.2.2. Size dependent sum kernel . . . 10
5.2.3. Product kernel . . . 15
6. Final conclusions, remarks and future prospects . . . 15
CRediT authorship contribution statement . . . 18
Declaration of competing interest . . . 18
Acknowledgement . . . 18
Appendix A. Methodology-II (Picard's iteration method) . . . 18
Appendix B. Validation of the proposed methodology . . . 19
Data availability . . . 19
References . . . 19

1. Introduction

The volume of milk used to make cheese is increasing globally, and control of milk coagulation, one of the first steps in cheese production, is essential to achieve high yield and consistent quality. Milk is a complex fluid composed of various proteins, fats, carbohydrates, vitamins, and minerals. Among its proteins, caseins are the most abundant, existing primarily in the form of casein micelles. In milk, casein proteins (alpha-casein, beta-casein, and kappa-casein) form micelles, which are spherical structures that hold these proteins together. The coagulation process initiates with the cleavage of milk proteins through the action of the proteolytic enzyme complex known as rennet. The rennet enzyme interacts with the natural colloidal particles called casein micelles present in milk, resulting in their aggregation to form a coagulum [1,2]. This coagulum is then cut to form curd. These curds can then be further processed to produce various types of cheese. Upon adding rennet to milk, it selectively acts on kappa-casein, a hairy structure found on the casein micelles. The rennet enzyme cleaves the kappa-casein molecules, which leads to the destabilization of the micelles and prompts their aggregation. Three consecutive processes occur during milk enzymatic coagulation treatment, two of which are important for mathematical modelling of the coagulation process. First of all, the casein micelles undergo proteolysis to produce unstable paracasein micelles and soluble peptides as shown below in Fig. 1. The coagulation of unstable paracasein micelles (of volumes x and y) and occurs at a rate $\beta(x, y, t)$, as illustrated in Fig. 2.

The coagulation process transforms liquid milk into a gel-like structure, which is cut and then separates into curds and whey over time. After the whey is drained, the remaining curds are used to produce the cheese. A number density function (number of particles in a differential volume) $\eta(x, t)$ can be used to study the evolving micelle size distribution during coagulation. The coagulation process of milk can be described using the population balance equation (PBE) [3] given by:

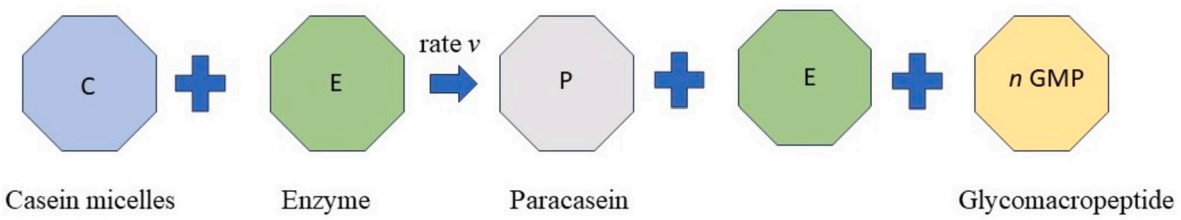

Fig. 1. Representation of first step (proteolysis) of rennet-induced coagulation process.

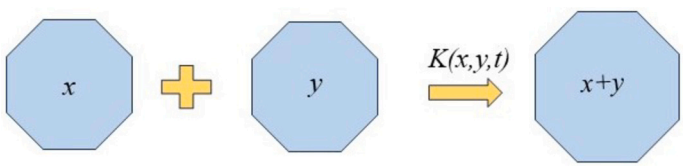

Fig. 2. Illustration of second step (coagulation to form coagulum) of rennet-induced coagulation process.

$$\frac{\partial \eta(x,t)}{\partial t} = K_1 g(x,0)\exp(-K_1 t) + \frac{1}{2}\int_0^x \beta(x-y,y,t)\eta(y,t)\eta(x,t)dx - \int_0^\infty \beta(x,y,t)\eta(x,t)\eta(y,t)dx, \tag{1}$$

with the initial conditions

$$g(x,0) = g_0(x), \quad \eta(x,0) = \eta_0(x), \ x \in]0,\infty[. \tag{2}$$

Here, $g(x,0)$ and $\eta(x,0)$ are initial concentration of the casein micelles and number density function of paracasein micelles having volume $x > 0$ at any time t, respectively. The fundamental phase of the enzymatic coagulation process, which is believed to exhibit first-order kinetics [3], is represented by the first term on the right side of equation (1), K_1 is the first-order rate constant for proteolysis, and the second term refers to the process by which casein micelles with volumes x and y merge to generate new casein micelles with volume $x+y$ at the rate $\beta(x,y,t)$. The rate $\beta(x,y,t)$ is known as the coalescence kernel, which is symmetric with respect to x and y. The third term describes the depletion of casein micelles having volumes x when merging with casein micelles with volume y.

1.1. Literature review and motivation

The progress over time of changes in particle characteristics brought about by nucleation, growth, aggregation, and breakage is described by population balance equations (PBEs). PBEs have a broad range of applications in almost all scientific domains such as chemical engineering [4], nuclear engineering [5], biomedical engineering [6], sprayed fluidized bed granulation [7], electrochemistry [8], and personalized medicine [9]. The second stage of the enzymatic coagulation process (1) (shown in Fig. 2) has been subjected to numerous studies that have examined different components including existence and uniqueness of solutions [10], scaling and self similarity [11] and gelation effect [12]. Gelation is a phase transition where the numerical method struggles to accurately preserve mass or volume, leading to challenges in modelling the coagulation process in cheese manufacturing. However, the nonlinear behaviour of the second stage of enzymatic coagulation restricts analytical solutions to only simple structured kernels [13–16]. Existing numerical approaches for the second stage of enzymatic coagulation process are available in literature such as method of moments [12], Discrete element method [17], Lattice Boltzmann method [18], finite volume schemes [19–21], and sectional methods [22,23]. Some recently developed semi-analytical approaches for aggregation and breakage models are provided in [24,25] and references therein. The merits and demerits of aforementioned methods have been discussed in detail in [21,26,27].

However, as per our knowledge, no analytical solutions are available for the combined first two stages of the enzymatic coagulation process. In the literature, different authors (refer to [3,28] and references therein) solved the combined first-two stages of enzymatic coagulation process by converting it to the moments form, which is given below:

$$\frac{d\mu_p(t)}{dt} = K_1\exp(-K_1 t)\int_0^\infty x^p g(x,0)dx + \frac{1}{2}\int_0^\infty\int_0^\infty \left[(x+x')^p - x^p - x'^p\right]\beta(x,x',t)f(x',t)f(x,t)dxdx'. \tag{3}$$

Here $\mu_p(t)$ is the p^{th} order moment. For $p=0$, the zeroth order moment can be captured which provides the total number of paracasein micelles in the system. Whereas for $p=1$, the first order moment can be derived which describes the total volume of paracasein micelles in the system. In the existing work, the authors used a Dirac delta function ($g(x,0)=\delta(x-1)$) centred at $x=1$ so that for all moments x^p is only evaluated at $x=1$ [3,29]. This restriction indicates that the unstable paracasein micelles formed during the initial phase of the enzymatic coagulation process have the same volume and size distributions cannot be modelled. In addition, traditional power series expansions were used to expand the integral moments which were dependent on many unknown variables and required additional calculations, leading to computational expense [30]. It is worth noting that power series expansions are not always the most efficient or accurate method for approximating functions or calculating integral moments. By using power series expansions, the integral moments can be approximated as a series of terms involving the unknown variables. This allows for simplification and potentially more manageable calculations. However, power series expansions typically involve an infinite number of terms, so truncating the series after a certain number of terms introduces some level of error into the approximation.

Compared to numerous numerical techniques that rely on meshes for computation, a variety of semi-analytic methods are also available in the literature for solving practical problems involving differential equations [31,32], integral equations [33], and integro-partial differential equations [34,35]. Some of semi-analytic techniques are B-spline methods [36–38], spectral techniques [39], special function based spectral technique [40], wavelet techniques [41,42].

In this work, our aim is to develop a meshfree approach based on the multistage Bernstein collocation method for the combined first-two stages of enzymatic coagulation process in order to track the macroscopic properties by converting the original equation (1) into the moments form (3). This approach demonstrates great flexibility and robustness in considering both Dirac delta and exponential initial conditions in order to model the first phase of the milk coagulation process. The use of exponential initial conditions enables us to analyse a diverse distribution of casein micelles with varying volumes across a broad range of the volume domain, making it a more practical approach. Moreover, the new approach offers a significant advantage over traditional numerical discretization methods in that it enables the solution without the need for unphysical restrictive assumptions such as linearization, discretization or perturbation. To enhance the understanding of the new approach, both existence of the solution and convergence are analyzed in detail. The accuracy of the new approach is compared against a finite volume method (FVM) and Picard's method. Particularly in areas with steep gradients, FVM may introduce numerical diffusion. Sharp gradients and minute details in the solution may not be

accurately captured due to this diffusion. As well, Picard's method is most effective for problems with weak nonlinearity. For strongly nonlinear problems, it may require an excessive number of iterations to reach convergence. Thus the practice of Picard's method is computationally expensive.

The rest of content of the article is outlined as follows: The existence of the solution is discussed in Section 2. In next Section 3, the basics of Bernstein polynomials and the detailed derivation of the multistage Bernstein collocation method for the enzymatic coagulation process (3) is presented. The convergence analysis is conducted in detail in Section 4. In Section 5, the new approach is tested against a finite volume scheme and Picard's method in order to check the accuracy and efficiency for different coagulation kernels. Next Section 6 is used to make some important remarks and conclusions related to the current study.

2. Existence theorem

In order to establish the existence theorem, the moment equation (3) can be rewritten into the following generalized differential equation

$$\frac{d\mu_p(t)}{dt} = M_p K_1 \exp(-K_1 t) + F(t, \mu_p(t)), \quad t \in [0, L) \text{ and } p = 0, 2, \tag{4}$$

where

$$F(t, \mu_p(t)) = \frac{1}{2} \int_0^\infty \int_0^\infty \left[(x + x')^p - x^p - x'^p \right] \beta(x, x', t) f(x', t) f(x, t) dx dx',$$

for the constant, sum kernel, and product kernels, where $M_p = \int_0^\infty x^p g(x, 0) dx$. The first order moment has exact solution $\mu_1(t) = M_1(1 - \exp^{-K_1 t}) + \mu_1(0)$ for every kernel β, where $\mu_1(0) = \int_0^\infty x f(x, 0) dx$. The initial value problem (IVP) (4) subject to the initial condition $\mu_p(0) = \int_0^\infty x^p f(x, 0) dx$ can be written in the following equivalent integral equation:

$$\mu_p(t) = M_p \left(1 - \exp(-K_1 t)\right) + \int_0^t F(s, \mu_p(s)) ds + \mu_p(0). \tag{5}$$

Some assumptions on the IVP (4) related to existence of the solution are as follows:

E1. $\mu_p(t) \in C[0, L] \cup C^1[0, L]$,
E2. $F(t, \mu_p(t)) \in C([0, L] \times C[0, L] \cup C^1[0, L], [0, \infty))$.

Theorem 2.1. ***(Index Theorem)*** *Let X be retract of real Banach space E, X_1 be bounded convex retract of X, and $U \subset X$ be nonempty open subset, such that $U \subset X_1$. If $T : \bar{X}_1 \to X$ is completely continuous operator, $T(X_1) \subset X_1$, such that there is no fixed point of T in $X_1 \setminus U$, then $i(T, U, X) = 1$.*

Proof. See [43]. □

The vector space $V = C[0, L]$ endowed with ordering $\mu_p(t) < \mu'_p(t)$, for all $t \in [0, L]$, and norm $\|\mu_p(t)\| = \max_{t \in [0,L]} |\mu_p(t)|$, form a Banach space. Let us define a cone H in the space V

$$H = \left\{ \mu_p \in V : \mu_p \geq 0, \min_{t \in [0,L]} \mu_p(t) \geq \lambda \|\mu_p(t)\| \right\}, \tag{6}$$

and an operator

$$S : H \to H, \tag{7}$$

such that

$$(S\mu_p)(t) = M_p \left(1 - \exp(-K_1 t)\right) + \int_0^t F(s, \mu_p(s)) ds + \mu_p(0). \tag{8}$$

The integral equation (5) has solution if and only if $\mu_p(t)$ solve the operator equation

$$\mu_p(t) = (S\mu_p)(t). \tag{9}$$

Lemma 2.1. *Let the conditions E1 and E2 hold, then the operator $S : H \to H$ is well defined and completely continuous.*

Proof. We have $\exp(-K_1 t) \leq 1$ for $t \in [0, L]$, then $1 - \exp(-K_1 t) \geq 0$ on $[0, L]$. Thus S is non-negative operator under the conditions E1 and E2. Since

$$(S\mu_p)(t) = M_p\left(1 - \exp(-K_1 t)\right) + \int_0^t F(s, \mu_p(s))ds + \mu_p(0), \tag{10}$$

implies

$$\min_{t\in[0,L]}(S\mu_p)(t) = \min_{t\in[0,L]}\left(M_p\left(1 - \exp(-K_1 t)\right) + \int_0^t F(s, \mu_p(s))ds + \mu_p(0)\right). \tag{11}$$

As $(S\mu_p)(t)$ is non-negative on $[0, L]$, thus there exist $0 < \lambda < 1$ such that

$$\min_{t\in[0,L]}(S\mu_p)(t) \geq \lambda \max_{t\in[0,L]}\left(M_p\left(1 - \exp(-K_1 t)\right) + \int_0^t F(s, \mu_p(s))ds + \mu_p(0)\right), \tag{12}$$

implies,

$$\min_{t\in[0,L]}(S\mu_p)(t) \geq \lambda\|(S\mu_p)(t)\|. \tag{13}$$

Thus S is well defined.
Now consider a sequence $\langle \mu_{p_n}(t)\rangle$ in H converges to $\mu_p(t) \in H$. Then there exists a constant l such that $\|\mu_{p_n}(t)\| < l$ for all n.
As F is continuous on $([0, L] \times [0, l])$, we have

$$\begin{aligned} |S\mu_{p_n}(t) - S\mu_p(t)| &= \left|\int_0^t F(s, \mu_{p_n}(s))ds - \int_0^t F(s, \mu_p(s))ds\right|, && (14)\\ &\to 0, \text{ as } n \to \infty, && (15)\\ &\Longrightarrow \|S\mu_{p_n}(t) - S\mu_p(t)\| \to 0, \text{ as } n \to \infty. && (16)\end{aligned}$$

Hence $S : H \to H$ is a continuous operator.
Let $G = \{\mu_p \in H : \|\mu_p(t)\| < e, e \text{ is positive constant}\}$ be bounded subset of H. For $\mu_p \in G$,

$$\begin{aligned} S\mu_p(t) &= M_p\left(1 - \exp(-K_1 t)\right) + \int_0^t F(s, \mu_p(s))ds + \mu_p(0), && (17)\\ &\leq \max_{t\in[0,L]}\left(M_p\left(1 - \exp(-K_1 t)\right) + \int_0^t F(s, \mu_p(s))ds + \mu_p(0)\right), && (18)\\ &< M_p + L\max_{(s,\mu_p)\in[0,T]\times[0,e]} f(s, \mu_p(t)) + \mu_p(0), && (19)\\ &\Longrightarrow S\mu_p(t) < \infty. && (20)\end{aligned}$$

Thus from Arzela-Ascoli theorem $S(G)$ is relatively compact subset of H, and the operator $S : H \to H$ is completely continuous. □

Lemma 2.2. *Suppose that E1 and E2 are satisfied and there exists a constant $d > M_p$, such that $f(s, \mu_p(s)) < \dfrac{d - M_p - \mu_p'}{L}$ then there exists one non-negative solution of the boundary value problem (4) subject to the initial condition $\mu_p(0) = \mu_p'$.*

Proof. Let $H_d = \{\mu_k \in H : \|m_p\| < d\}$ be open subset of H. We have to show that $S\bar{H}_d \subset \bar{H}_d$. For $\mu_p \in \bar{H}_d$

$$\begin{aligned} S\mu_p(t) &= M_p(1 - \exp(-K_1 t)) + \int_0^t F(s, \mu_p(s))ds + \mu_p', && (21)\\ &< M_p + \frac{d - M_p - \mu_p'}{L}\max_{t\in[0,L]}\int_0^t ds + \mu_p', && (22)\\ &\Longrightarrow \|S\mu_p\| < d. && (23)\end{aligned}$$

Since $|\mu_p(t)| < d$ only on H_d, not on the boundary $\partial H_d = \bar{H}_d \setminus H_d$. Thus there is no fixed point on boundary ∂H_d. Using Theorem 2.1, $i(S, H_d, H) = 1$. Thus the IVP (4) has one non-negative solution. □

3. Basics of multistage Bernstein polynomials

3.1. Bernstein polynomials

The Bernstein polynomials of degree m on the interval $[0, 1]$ are given by

$$B_{i,m}(t) = \binom{m}{i} t^i (1-t)^{m-i}, \quad i = 0, 1, 2, \cdots, m,$$

where

$$\binom{m}{i} = \frac{m!}{i!(m-i)!}.$$

These Bernstein polynomials can be generalized to any interval for the microscopic investigation of any signal (solution).

3.2. Generalized Bernstein polynomials

The Bernstein polynomials can be generalized on any general interval $[a, b]$ by normalizing t on $[a, b]$ with $t = \frac{x-a}{b-a}$, as follows

$$B_{i,m}(x) = \binom{n}{r} \left(\frac{x-a}{b-a}\right)^i \left(1 - \left(\frac{x-a}{b-a}\right)\right)^{m-i}, \quad i = 0, 1, 2, \cdots, m.$$

3.3. Bernstein function approximation

The approximate solution using least degree Bernstein basis polynomials may not converge using the conventional collocation technique on an interval of large length. The interval $[0, L]$ can be divided into n sub-intervals of equal length h

$$[0 = t_0, t_1], [t_1, t_2], \ldots [t_{n-1}, t_n = L],$$

to get out of this problem. On each sub-interval the Bernstein basis polynomials can be used to approximate a function $f(t) \in L_2[0, L]$ as follows

$$\begin{aligned} f(t) = f_m^n(t) \cong & \begin{cases} f_m^1(t) = \sum_{i=0}^{m} c_i^1 B_{i,m}^1(t) = C_1^T B_1(t), & t \in [0 = t_0, t_1], \\ f_m^2(t) = \sum_{i=0}^{m} c_i^2 B_{i,m}^2(t) = C_2^T B_2(t), & t \in [t_1, t_2], \\ \qquad\qquad\qquad \vdots \\ f_m^n(t) = \sum_{i=0}^{m} c_i^n B_{i,m}^n(t) = C_n^T B_n(t), & t \in [t_{n-1}, t_n = L], \end{cases} \\ & = [C_1^T, C_2^T, \ldots, C_n^T] \begin{bmatrix} B_1(t) \\ B_2(t) \\ \vdots \\ B_n(t) \end{bmatrix}, \\ & = C^T B, \end{aligned} \tag{24}$$

where, the coefficient of function approximation and the corresponding Bernstein basis on j^{th} interval is given by

$$C_j = [c_0^j, c_1^j, \ldots, c_m^j]^T, \quad B_j(t) = [B_{0,m}^j(t), B_{1,m}^j(t), \ldots, B_{m,m}^j(t)]^T, \quad j = 1, 2, \ldots, n. \tag{25}$$

3.4. Spline based multi-stage Bernstein collocation method

This section develops a scheme to find the numerical solution of equation (3) to approximate the enzymatic coagulation. To find the numerical solution of (3), the combined equation of first two stages of coagulation process, that is, the moment equation (3) is used and can be written as the following generalized differential equation

$$\frac{d\mu_p(t)}{dt} = M_p K_1 \exp(-K_1 t) + F(t, \mu_p(t)), \quad t \in [0, L) \text{ and } p = 0, 2, \tag{26}$$

for the constant kernel, sum kernel, and the product kernel, where $\mu_p(0) = \mu_p'$. Using equation (24), differential equation (26) can be expressed in the following algebraic equation

$$C^T B' - M_p K_1 \exp(-K_1 t) - F(t, C^T B) = 0, \tag{27}$$

where $\mu_p(t) = C^T B$, and $B' = [B'_1(t), B'_2(t), \ldots, B'_n(t)]$. The function $\mu_p(t)$ is divided into n piece-wise series and each series consists $m+1$ unknown Bernstein coefficients, that is, there is need to find the values of $n(m+1)$ unknown Bernstein coefficients in order to find the approximate solution. The proposed methodology deals the equation (26) piece-wise on sub-intervals $[t_{i-1}, t_i], \quad i = 1, 2, \ldots, n$ of equal length h of the interval $[0, L)$. Now, we introduce here m collocation points on the first sub-interval $[0 = t_0, t_1]$, given by

$$t^1_{0i} = t_0 + \frac{i}{m} h, \quad i = 1, 2 \ldots m. \tag{28}$$

The collocation points (28) transform the equation (27) into m nonlinear algebraic equations on the sub-interval $[0 = t_0, t_1]$, given by

$$C_1^T B'_1(t^1_{0i}) - M_p K_1 \exp(-K_1 t^1_{0i}) - F(t^1_{0i}, C_1^T B_1(t^1_{0i})) = 0. \tag{29}$$

The equation (29) together with an initial condition $\mu_p(0) \cong C_1^T B'_1(0) = \mu'_p$ produces $m+1$ nonlinear algebraic equations in contrast to $m+1$ unknown Bernstein coefficients. The solution of these algebraic equation with suitable method provides the required solution of (4) on the interval $[t_0, t_1]$. In a similar fashion, we choose $m-1$ collocation points, given by

$$t^j_{j-1i} = t_{j-1} + \frac{i}{m-1} h, \quad i = 1, 2, ..., m-1, \tag{30}$$

on the jth sub-interval for $2 \le j \le n$. These collocation points produce $m-1$, nonlinear algebraic equations

$$C_j^T B'_j(t^j_{j-1i}) - M_p K_1 \exp(-K_1 t^j_{j-1i}) - F(t^j_{j-1i}, C_j^T B_j(t^j_{j-1i})) = 0, \tag{31}$$

on the respective sub-interval. Using the procedure of spline method, there exist a pair of algebraic equations

$$C_j^T B_j(t_{j-1}) = M_p^*, \tag{32}$$

$$C_j^T B'_j(t_{j-1}) = M_p^{**}, \tag{33}$$

in order to maintain the continuity and the smoothness of the solution at left partition node of the next concern sub-interval. Here M_p^* and M_p^{**} are the values of approximate value of $\mu_p(t)$ and its derivative at t_{j-1} on the previous sub-interval. Combination of the equations (31) and the pair of algebraic equation (32) and (33) produces $m+1$ nonlinear algebraic equations. We solve these algebraic equations for the respective unknown Bernstein coefficients. This complete process provides the required solution on the interval $[0, L)$.

4. Convergence analysis

Theorem 4.1. *Consider μ_p be $\alpha+1$ times continuously differentiable function, and V be the space of the functions generated with the Bernstein basis $B_j = \{B^j_{0,\alpha}(t), B^j_{2,\alpha}(t), \ldots, B^j_{\alpha,\alpha}(t)\}$. Let $\mu_{p_\alpha} \in V$ be the best fit of μ_p on the jth sub-interval of the interval $[0, L]$, then the error bound is*

$$\|\mu_p(t) - \mu_{p_\alpha}(t)\| \le h^{\alpha+1} \frac{N}{(\alpha+1)!}, \tag{34}$$

where $N = \max_{t \in [t_{j-1}, t_j]} |\mu_p^{(\alpha+1)}(t)|$, and $h = t_j - t_{j-1}$.

Proof. Consider the equivalent α-degree Taylor's polynomial $\mu_{p1}(t)$ of $\mu_p(t)$ in terms of $\mu_{p_\alpha}(t)$ as follows

$$\mu_p(t) = \sum_{i=0}^{\alpha} \frac{(t - t_{j-1})^i}{i!} \mu_{p_\alpha}{}^{(i)}(t_{j-1}) \cong \mu_{p_\alpha}(t), \tag{35}$$

and the Taylor's theorem state that

$$\left| \mu_p(t) - \sum_{i=0}^{\alpha} \frac{(t - t_{j-1})^i}{i!} \mu_{p_\alpha}{}^{(i)}(t_{j-1}) \right| = \left| \mu_p^{(\alpha+1)}(\xi) \frac{(t - t_{j-1})^{\alpha+1}}{(\alpha+1)!} \right|, \tag{36}$$

$$< \max_{t \in [t_{j-1}, t_j]} \left| \mu_p^{(\alpha+1)}(\xi) \frac{(t - t_{j-1})^{\alpha+1}}{(\alpha+1)!} \right|, \tag{37}$$

$$\le h^{\alpha+1} \frac{N}{(\alpha+1)!}, \tag{38}$$

implies

$$\|\mu_p(t) - \mu_{p_\alpha}(t)\| \le h^{\alpha+1} \frac{N}{(\alpha+1)!}. \tag{39}$$

Thus the approximation $\mu_{p_\alpha}(t)$ converges to $\mu_k(t)$ uniformly as $h \to 0$ or $\alpha \to \infty$. □

Theorem 4.2. *Suppose the function $f(t, \mu_p(t))$ is a Lipschitz continuous, i.e. there exists a constant $\mathcal{L}$ such that*

$$|f(t, \mu_p(t)) - f(t, \mu_p*(t))| \leq \mathcal{L}|\mu_p - \mu_p*|, \forall\, t \in [t_{j-1}, t_j] \text{ and } \mu_p, \mu_p* \in V. \tag{40}$$

Then the approximate solution $\mu_{p_\alpha}(t)$ of the IVP (4) subject to the boundary condition $\mu_p(0) = \mu_p'$ converges uniformly to the exact solution $\mu_p(t)$ as $h \to 0$ or $\alpha \to \infty$.

Proof. Suppose $\mu_p \in V$, we have

$$S\mu_p(t) = M_p(1 - \exp(-K_1 t)) + \int_{t_{j-1}}^{t_j} F(s, \mu_p(s))ds + \mu_p(0). \tag{41}$$

Since approximation $\mu_{p_\alpha}(t) \in V$, then

$$S\mu_{p_\alpha}(t) = M_p(1 - \exp(-K_1 t)) + \int_{t_{j-1}}^{t_j} F(s, \mu_{p_\alpha}(s))ds + \mu_p(0). \tag{42}$$

Thus from equation (41) and (42), we have

$$\begin{aligned} |S(\mu_p - \mu_{p_\alpha})(t)| &= \int_{t_{j-1}}^{t_j} \left| F(s, \mu_p(s)) - F(s, \mu_{p_\alpha}(s)) \right| ds, \\ &\leq \mathcal{L} \int_0^t \left(|\mu_p(s) - \mu_{p_\alpha}(s)| \right) ds, \end{aligned}$$

implies

$$\max_{t\in[t_{j-1},t_j]} |S(\mu_p - \mu_{p_\alpha})(t)| \leq \max_{t\in[t_{j-1},t_j]} \left(\mathcal{L}h|\mu_p(s) - \mu_{p_\alpha}(s)| \right). \tag{43}$$

Now using the result of Theorem 4.1, we have

$$\begin{aligned} \|S(\mu_p - \mu_{p_\alpha})(t)\| &\leq \mathcal{L}h\|\mu_p(s) - \mu_{p_\alpha}(s)\|, \\ &< \mathcal{L}h^{\alpha+2}\frac{N}{(\alpha+1)!}. \end{aligned} \tag{44}$$

This completes the proof. □

5. Numerical testing and discussion

The proposed method has been subject to test against finite volume scheme, and Picard's method for the numerical solutions of moments equations corresponding to non-gelling constant kernels, sum kernels, and the product kernels in terms of residual error

$$Rw = \left| \frac{d\mu_p(t)}{dt} - M_p K_1 \exp(-K_1 t) + F(t, \mu_p(t)) \right|, \quad t \in [0, T) \text{ and } p = 0, 2, \tag{45}$$

and absolute error norm

$$e = |Exact - \text{BCM}(N)|. \tag{46}$$

The definitions of Avg_{Rw} and End_{Rw} for residual error Rw have been defined by

$$Avg_{Rw} = \frac{1}{n}\sum_{i=1}^{n} Rw(t_i), \quad \text{and} \quad End_{Rw} = Rw_{t_n}, \tag{47}$$

where n is number of test point over the time period, and t_i is i^{th} test point. The maximum relative error norm $\rho_\infty = \max_{t\in[0,L]} \left| \frac{FVS - Approximate}{FVS} \right|$ is also used to validate the methods against existing finite volume scheme.

All the computational works are performed on Maple-18 and the results are plotted on MATLAB-2017b on the PC with configuration (CPU Core(TM) i5-8285U @1.60 GHz, and 8 GB RAM). It is important to note that all the calculations of the normalized moments are done for dimensionless volume and time. The normalization of the moments is done by dividing with the initial values of their respective moments.

Table 1
Error analysis of the moments for constant kernel without proteolysis process.

	μ_0			μ_1		
t	Exact	$N = 8$	e	Exact	$N = 8$	e
0	1	1	0	1	1	0
0.306455	0.867131	0.867131	3.1E-09	1	0.999999	1.1E-15
0.817213	0.709921	0.709921	1.9E-09	1	0.999999	2.1E-15
1.327971	0.600966	0.600966	1.3E-09	1	0.999999	9.9E-16
1.940881	0.507501	0.507501	1.3E-09	1	0.999999	1.3E-15

Table 2
Error analysis of the moments for sum kernel without proteolysis process.

	μ_0			μ_1		
t	Exact	$N = 10$	e	Exact	$N = 10$	e
0	1	0.999999	2.2E-15	1	0.999999	2.3E-15
0.1903	0.826711	0.826711	1.8E-13	1	0.999999	3.7E-15
0.5076	0.601938	0.601938	1.3E-13	1	0.999999	3.4E-15
0.8248	0.438322	0.438322	6.3E-14	1	1.000000	4.4E-16
1.2055	0.299542	0.299542	4.2E-14	1	0.999999	7.2E-15

5.1. Coagulation without proteolysis process

In this part, we demonstrate the implementation of a recently formulated method for solving the moment equation of a pure coagulation equation. This equation can be readily obtained by substituting $K_1 = 0$ into the given equation (3) which takes the following form:

$$\frac{d\mu_k(t)}{dt} = \frac{1}{2}\int_0^\infty \int_0^\infty \left[(x+x')^k - x^k - x'^k\right]\beta(x,x',t)f(x',t)f(x,t)dxdx', \quad t \in [0,L) \text{ and } k = 0,1. \tag{48}$$

First we validate the results obtained by the new approach with the exact solutions of the moments for a pure coagulation equation provided in [44] and references therein. For performing the testing, a size-independent and size-dependent kernels are considered corresponding to an initial condition $f(x,0) = e^{-x}$. The testing of the accuracy is done in terms of the first two moments ($p = 0$ and 1).

5.1.1. Size-independent constant kernel

The closed form solution of moments for $k = 0$, and 1 for a pure coagulation equation for the constant kernel $\beta(x,y) = 1$ provided in the literature [44] are

$$\mu_0 = \frac{2}{2+t}, \text{ and } \quad \mu_1 = 1. \tag{49}$$

To test the validity of the proposed methodology, equation (48) has been solved for constant kernel and the results obtained are demonstrated qualitatively in Table 1.

Table 1 clearly illustrates that the numerical approximations by BCM at $N = 8$ match very well with the closed-form solution (Exact) to a significant degree. This shows that the Bernstein collocation method approximated the zeroth and first order moments with high precision. Table 1 shows that the accuracy of the BCM in terms of the residual errors in the first two order moments is high, which shows the potential of the new approach.

5.1.2. Size-dependent sum kernel

Now let us consider a more challenging size-dependent sum kernel $\beta(x,y) = x + y$ with an exponential initial condition. Once again the closed form moments solution of the equation (48) with sum kernel $\beta(x,y) = x + y$ given in [44] are listed below:

$$\mu_0 = e^{-t}, \text{ and } \quad \mu_1 = 1. \tag{50}$$

The quantitative results for the moments are shown Table 2 for a sum kernel. The results estimated using the BCM numerical approximations match with the closed form solution with a high precision illustrated in Table 2. Table 2 demonstrates that the accuracy of the proposed technique in terms of the residual errors. It shows that the errors in the zeroth and first order moments are of the order 10^{-13} and 10^{-15}, respectively for $N = 10$.

Table 3
Error analysis of the moments for constant kernel.

	$K_1 = 5$				$K_1 = 10$			
	Avg_{Rw}		End_{Rw}		Avg_{Rw}		End_{Rw}	
$\mu_p(t)$	BCM(6)	BCM(8)	BCM(6)	BCM(8)	BCM(6)	BCM(8)	BCM(6)	BCM(8)
$\mu_0(t)$	0.018970	0.003503	7.8E-06	3.5E-07	0.301104	0.077546	4.4E-07	4.4E-08
$\mu_1(t)$	0.037608	0.001654	7.0E-06	2.5E-07	0.278630	0.079749	4.4E-07	6.0E-08
$\mu_2(t)$	0.056822	0.010533	8.5E-06	3.1E-07	0.526254	0.175974	6.9E-07	1.3E-07

5.2. Coagulation with proteolysis process

Here we test the accuracy of the new approach by considering the coagulation with the proteolysis process. The comparison is conducted for an arbitrary exponential initial condition $f(x,0) = e^{-x}$ and $g(x,0) = f(x,0)$ for the purpose of testing. However, both approaches are flexible and robust to work with any form of $g(x,0)$. The numerical scheme of Picard's iterative method is presented in Appendix A.

5.2.1. Constant kernel

We begin the testing of the new approach by considering a constant kernel $\beta(x,y) = 1$. For this case, we have found the closed forms of the first and second moments using Picard's method. Few order moments equations (linear in nature) give exact closed form solutions depending on the kind of aggregation kernel considered. For other moments (specifically zeroth moment), nonlinear expressions are obtained and the series solutions are obtained by implementing the multistage Bernstein collocation method (BCM) and Picard's method. To check the extent of accuracy of the numerical approximates, residual errors (45) are estimated by considering different number of series terms. The simulations are run until time $t = 2$ for $K_1 = 5$ and $K_1 = 10$.

Figs. 3(a) and 4(a) demonstrate that the accuracy of the zeroth order moments using different techniques. Figures reveal that the BCM solutions match very well with the exact solution and FVS [45], whereas the accuracy of Picard's method deteriorates after time $t = 0.4$. The relationship between the accuracy of the solutions and the value of α, which represents the degree of Bernstein polynomials in BCM is readily apparent. Theorem 4.2 states, as the degree of the Bernstein polynomials α increases, the accuracy of the solutions improves considerably (*cf.* Table 3). However, it is important to note that increasing the number of iterations in Picard's method also leads to a rise in computational complexity.

In addition, for $K_1 = 5$ and $K_1 = 10$, Figs. 3(c) and 4(c) illustrate the total mass in the system (μ_1), and all methods show equal accuracy, qualitatively. It can be seen that the total mass of paracasein micelles increases due to enzymatic proteolysis and then remains constant as coagulation progresses. We also analyse the effect of the values of K_1 on the proteolysis process. While considering $K_1 = 10$, the proteolysis process experiences a reduced duration, completing by $t = 0.61$ (as depicted in Fig. 4(c)). Furthermore, the second order moments presented in Figs. 3(e) and 4(e) are estimated by all methods with equal precision, with which one can analyse the variance of particle size over the process.

The qualitative analysis of different order moments illustrated in Figs. 3 and 4 does not allow us to visualise the accuracy clearly. Therefore, the residual errors are plotted that demonstrate the accuracy of the BCM approach against the Picard's method (refer to Figs. 3(b), 3(d), 3(f), 4(b), 4(d) and 4(f)). The quantitative residual errors computed for different order moments demonstrate the reliability of the proposed method (BCM) and explain the convergence of the methodology. The residual errors in different order moments are computed and listed in Table 3 for different values of K_1. Table shows that the values of K_1 have a significant effect on the residual errors, that is, for larger value of $K_1 = 10$, the residual errors in the moments are higher than the residual errors estimated corresponding to $K_1 = 5$.

5.2.2. Size dependent sum kernel

Now we consider a more complex size dependent sum kernel $\beta(x,y) = x + y$ with an exponential initial condition. Due to heavy size dependency, it is only feasible to find the close solutions of the first order moment. However, the zeroth and second order moments equations are very complex and very challenging to solve analytically. Therefore, the BCM and Picard's method are used to solve the equations corresponding to these moments, and the solutions are compared with the FVS. All the calculations are done for the time interval $[0, 1.2]$.

The qualitative comparison of BCM and Picard's method against the FVS is demonstrated in Figs. 5 and 6 for $K_1 = 5$, and $K_1 = 10$, respectively. It can be seen that both zeroth and first order moments are equally well computed by BCM and Picard's method and match well with the FVS (see Figs. 5(a), 6(a), 5(c) and 6(c)). In addition, the second order moments demonstrated in Figs. 5(e) and 6(e) show that the second order moments are almost equally well approximated by both the methods and deviate slightly from the FVS result. The qualitative residual error analysis is done for different values of K_1 as shown in Figs. 5(b), 5(d), 5(f), 6(b), 6(d) and 6(f). It can be seen that overall the BCM shows higher quality solutions for the moments than the Picard's method. The proteolysis time is considered to be the time when the proteolysis reaction is completed. It is seen when the first order moment becomes constant. For the proteolysis constant $K_1 = 5$ the first order moment reaches the coagulation point after $t = 1$, whereas it reaches to coagulation point at $t = 0.61$ for $K_1 = 10$ (see Figs. 5(c), and 6(c)). This shows that the large value of K_1 decreases the duration of proteolysis process. The numerical results of Picard's iterative techniques for gelling sum kernel are provided at eight iterations. The gelling sum kernel describes the rate at which the paracasein micelles aggregate under enzymatic action, with the coagulation rate being

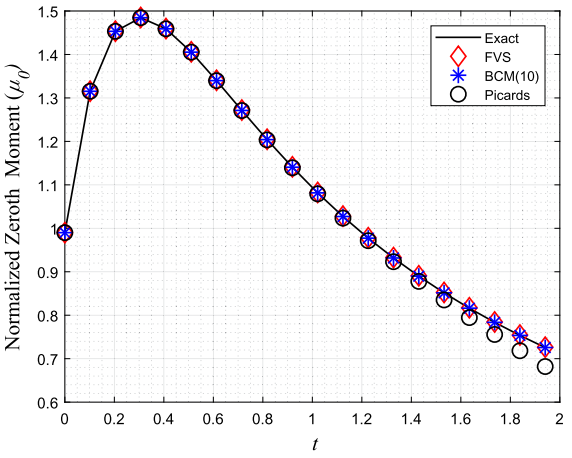

(a) μ_0 for $N = 10$

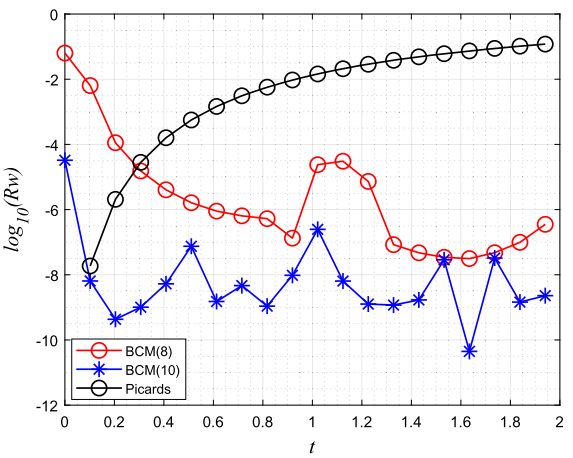

(b) $log_{10}(Rw)$ for μ_0 with $N = 8$ and 10

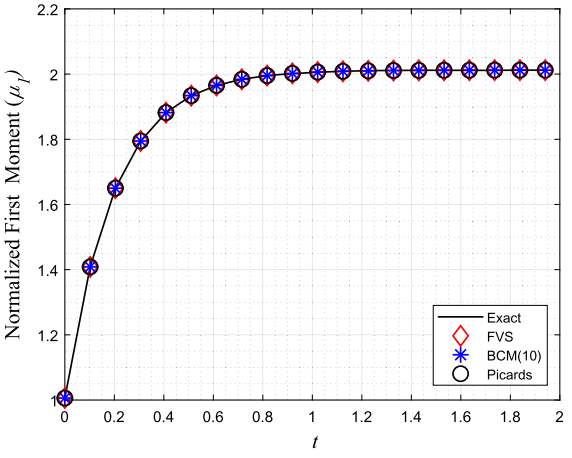

(c) μ_1 for $N = 10$

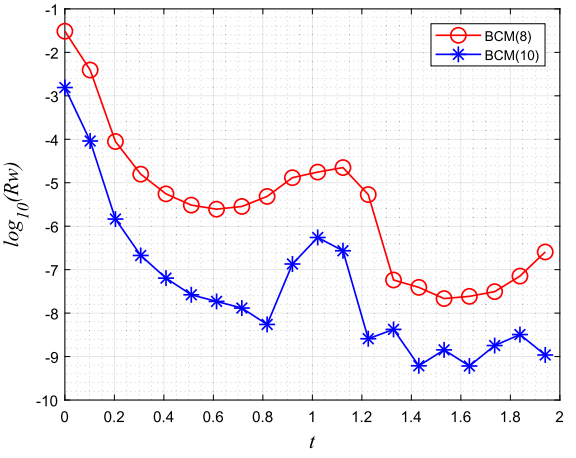

(d) $log_{10}(Rw)$ for μ_1 with $N = 8$ and 10.

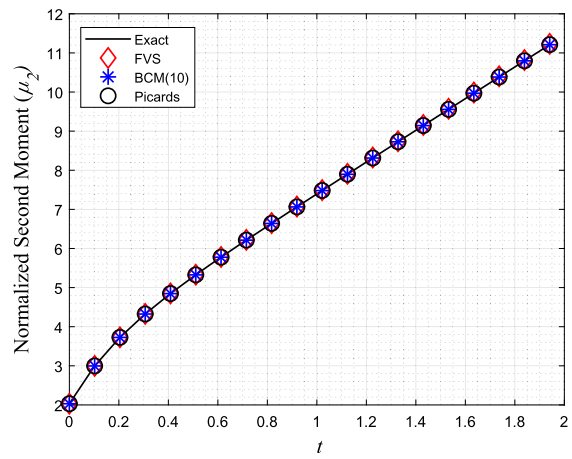

(e) μ_2 for $N = 10$

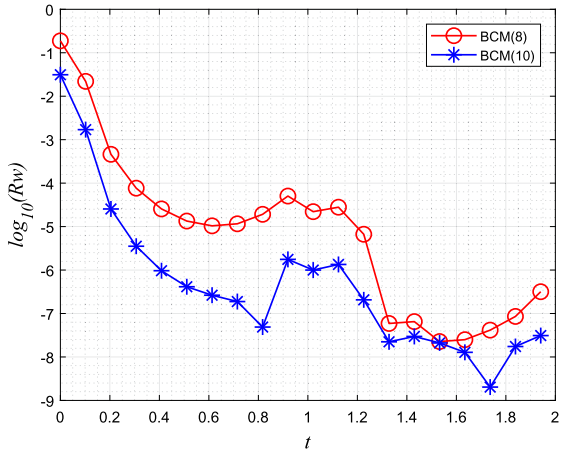

(f) $log_{10}(Rw)$ for μ_2 with $N = 8$ and 10

Fig. 3. Testing of different moments and their residual errors for constant kernel $\beta(x, y) = 1$ with $K_1 = 5$.

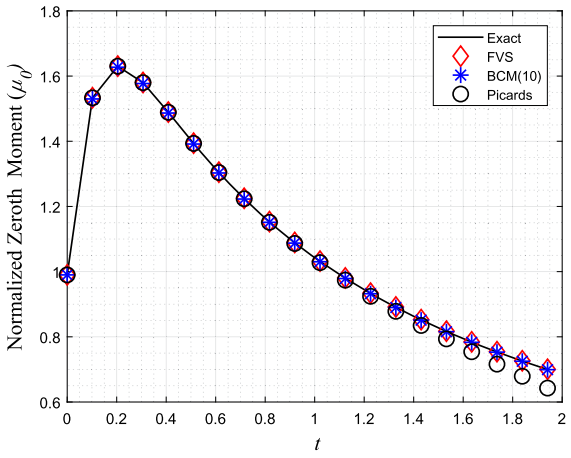

(a) μ_0 for $N = 10$

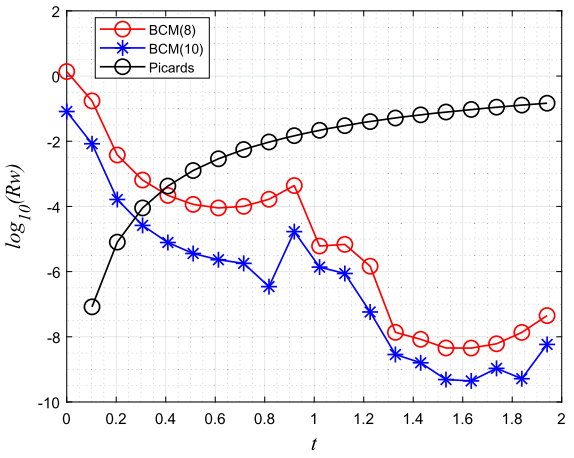

(b) $log_{10}(Rw)$ for μ_0 with $N = 8$ and 10

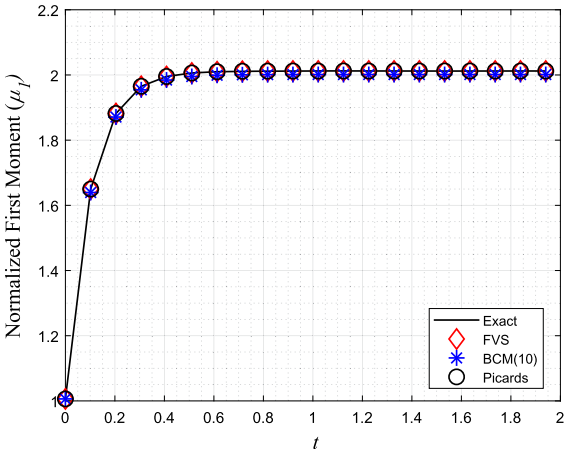

(c) μ_1 for $N = 10$

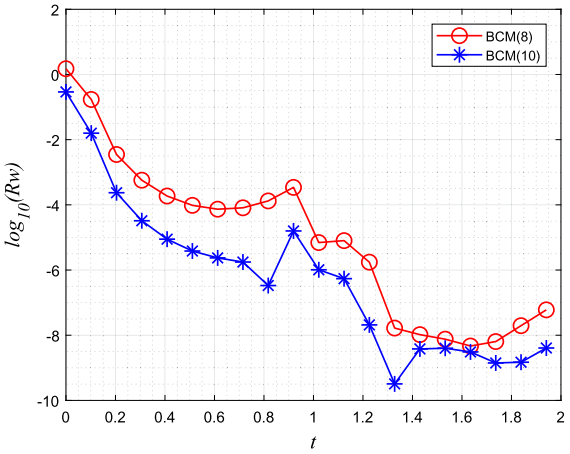

(d) $log_{10}(Rw)$ for μ_1 with $N = 8$ and 10

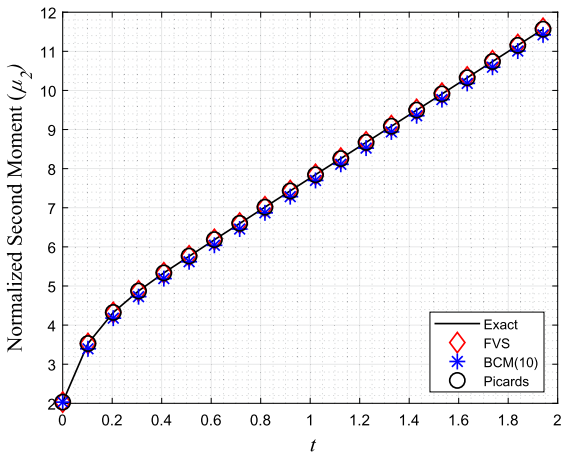

(e) μ_2 for $N = 10$

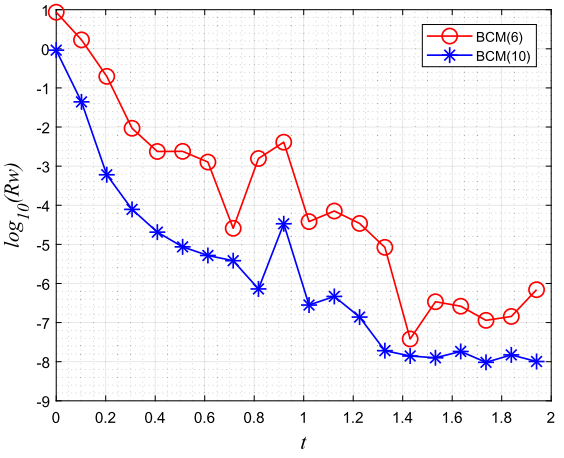

(f) $log_{10}(Rw)$ for μ_2 with $N = 8$ and 10

Fig. 4. Testing of different moments and their residual errors for constant kernel $\beta(x, y) = 1$ with $K_1 = 10$.

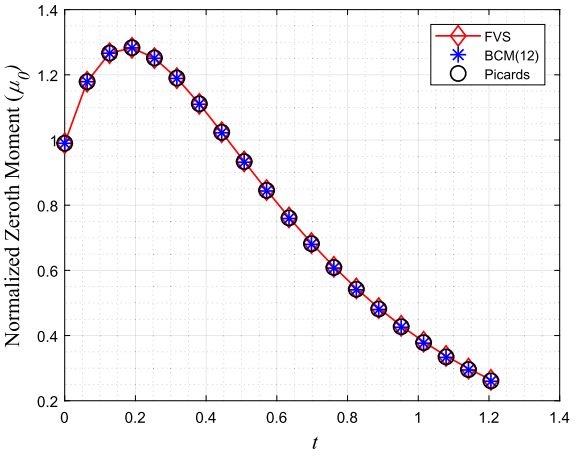

(a) μ_0 for $N = 12$

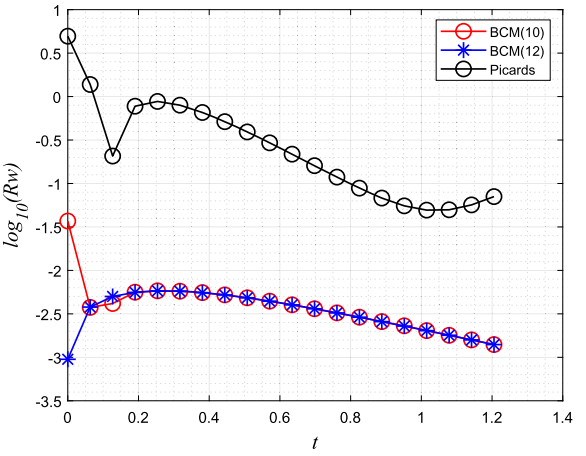

(b) $log_{10}(Rw)$ for μ_0 with $N = 10$ and 12

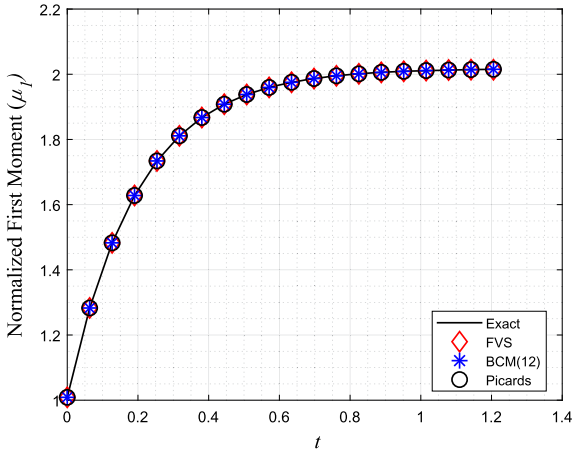

(c) μ_1 for $N = 12$

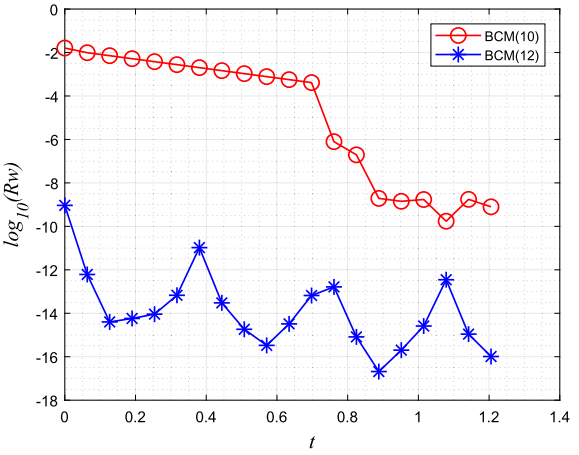

(d) $log_{10}(Rw)$ for μ_1 with $N = 10$ and 12

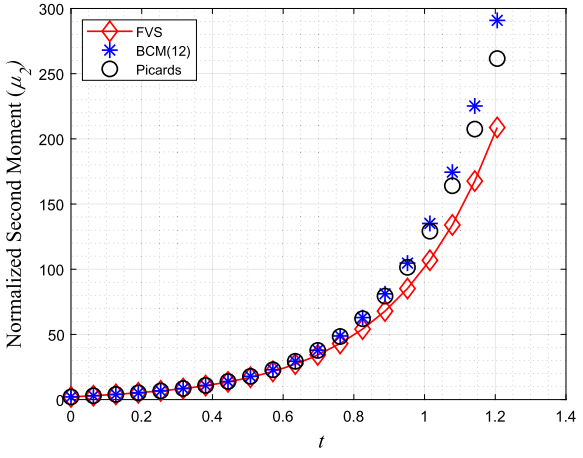

(e) μ_2 for $N = 12$

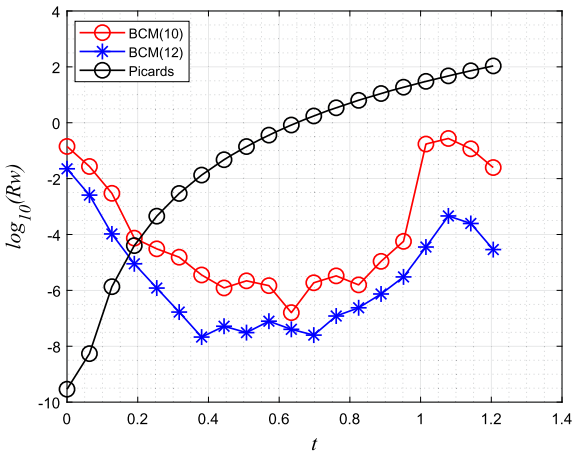

(f) $log_{10}(Rw)$ for μ_2 with $N = 10$ and 12

Fig. 5. Testing of different moments and their residual errors for sum kernel $\beta(x, y) = x + y$ with $K_1 = 5$.

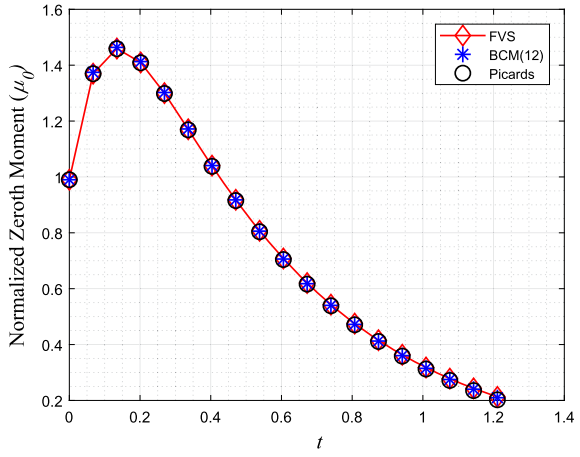

(a) μ_0 for $N = 12$

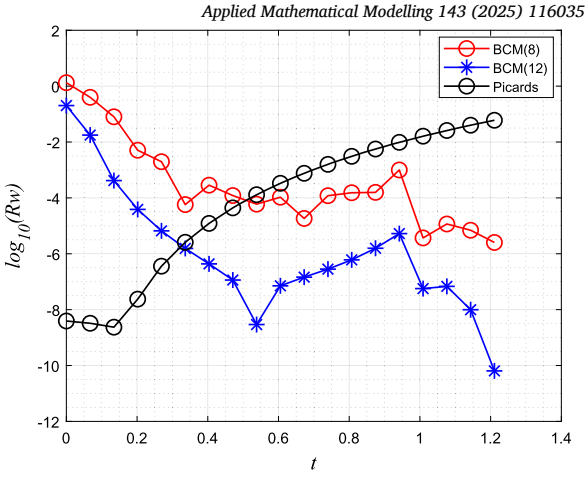

(b) $log_{10}(Rw)$ for μ_0 with $N = 8$ and 12

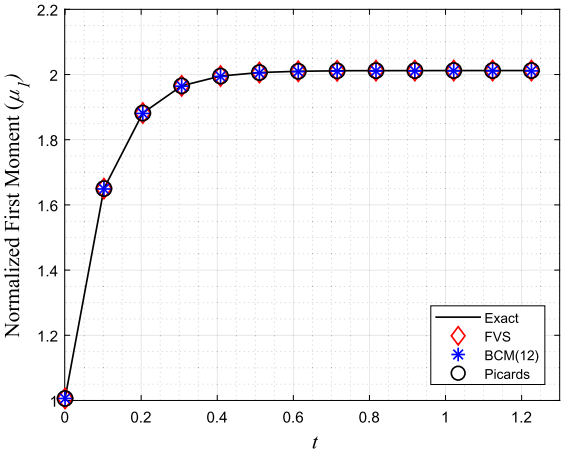

(c) μ_1 for $N = 12$

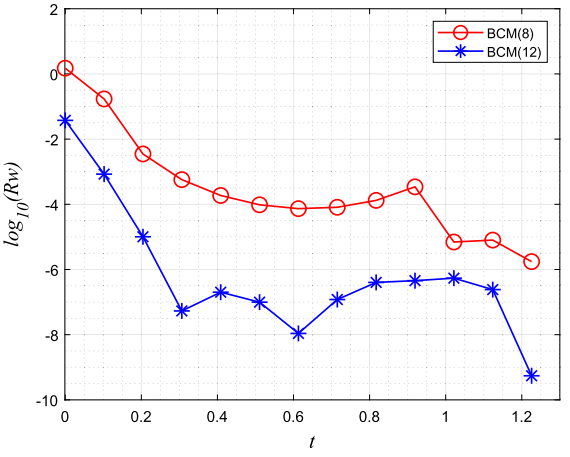

(d) $log_{10}(Rw)$ for μ_1 with $N = 8$ and 12

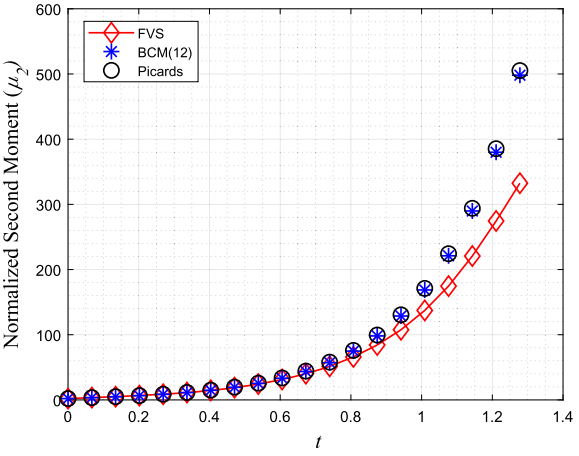

(e) μ_2 for $N = 12$

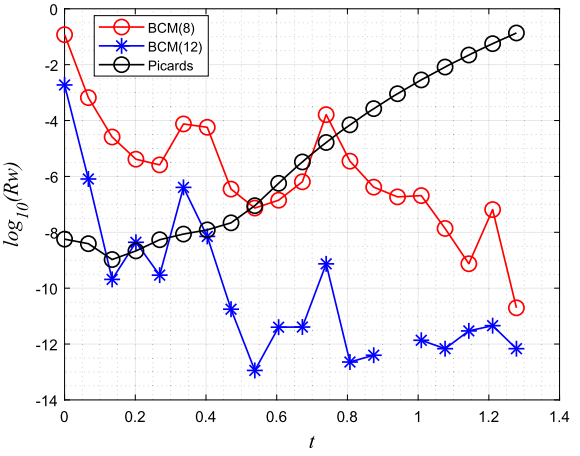

(f) $log_{10}(Rw)$ for μ_2 with $N = 8$ and 12

Fig. 6. Testing of different moments and their residual errors for sum kernel with $K_1 = 10$.

Table 4
Closeness of the proposed methods with FVS in terms of relative error (ρ_∞).

	Sum Kernel			
	$K_1 = 5$		$K_1 = 10$	
$\mu_p(t)$	BCM(12)	Picards	BCM(12)	Picards
$\mu_0(t)$	1.1E-02	1.3E-02	1.3E-02	4.9E-02
$\mu_1(t)$	6.7E-04	6.7E-04	7.0E-04	2.7E-05
$\mu_2(t)$	3.9E-01	2.5E-01	5.1E-01	5.1E-01

Table 5
Error analysis of the moments for sum kernel.

	$K_1 = 5$						$K_1 = 10$					
	Avg_{Rw}		End_{Rw}		RT		Avg_{Rw}		End_{Rw}		RT	
$\mu_p(t)$	BCM(8)	BCM(12)	BCM(8)	BCM(12)	BCM(8)	BCM(8)	BCM(8)	BCM(12)	BCM(8)	BCM(12)	BCM(8)	BCM(8)
$\mu_0(t)$	0.013369	0.003618	1.3E-03	1.4E-04	0.98 sec	1.37 sec	0.095563	0.011577	2.5E-06	6.4E-11	1.26 sec	1.54 sec
$\mu_1(t)$	0.002079	2.6E-06	7.8E-06	1.4E-08	0.93 sec	1.34 sec	0.083736	0.001923	6.0E-08	4.0E-09	1.39 sec	2.5 sec
$\mu_2(t)$	0.131664	0.001370	4.6E-05	1.0E-06	1.40 sec	1.46 sec	0.379124	0.032892	9.6E-06	6.3E-06	1.54 sec	1.64 sec

proportional to the sum of the sizes of the interacting particles. Picard's method can produce more precise results with increase in the number of iterations, but with a high computational cost. The computation cost is provided in terms of CPU run time (RT) for $h = 0.35$ in the Table 5. In comparison to Picard's method, the BCM produces high quality results with low computational cost. The quantitative errors in the moments are listed in Table 5 for $K_1 = 5$, and $K_1 = 10$ and shows similar behaviour as previous cases, that is, with $K_1 = 10$, the residual errors are higher compared to $K_1 = 5$ and can be reduced to a desired level by considering large values of N as demonstrated in table.

Table 4 demonstrates that the proposed methods are sufficiently close to the existing finite volume scheme, serving as a viable alternative. Additionally, Table 5 shows that the approximate solutions align well with the proposed model.

5.2.3. Product kernel

We enhance the testing by considering a more complex product kernel of the form $\beta(x, y) = xy$. For this particular case, linear differential equations are obtained for the zeroth and first order moments, and therefore exact solutions for both moments are obtained. However, for the second order moments, a non-linear differential equation is formed which cannot be solved analytically. Similar to the previous cases, the accuracy of both BCM and Picard's method are compared against the FVS for different values of K_1.

The comparison of BCM, Picard's method and FVS is demonstrated in Figs. 7, and 8 for $K_1 = 5$, and $K_1 = 10$, respectively. The zeroth and first order moments predicted by BCM and Picard's method show good precision and match very well with the FVS results as shown in Figs. 7(a), 7(c), 8(a) and 8(c). In addition, the second order moments estimated by both approaches are compared with FVS in Figs. 7(e) and 8(e). The results show that Picard's method shows deviation very early compared to BCM. The accuracy of Picard's method is highly dependent on the number of series terms considered. Adding more series terms will make the calculation computationally expensive. The precision of the BCM can easily be increased by considering high degree of Bernstein polynomials at a lower computational cost.

The residual errors in different moments are also estimated using the BCM for $K_1 = 5$, and $K_1 = 10$. The results are graphical depicted in Figs. 7(b), 7(f), 8(b) and 8(f). The results show similar behaviour as the previous cases, that is, for very short times Picard's method performs better than the BCM, however, for the longer time domain, the BCM shows lesser residual errors in the moments compared to the Picard's method. These residual errors are quantified and listed in Table 6 which shows that the BCM approach is very robust and reliable to capture these macroscopic properties with high precision at a low computational expense.

From above results and discussion, we can conclude that irrespective of the form of the equations (linear or nonlinear) of the moments, the BCM has the tendency to estimate the microscopic properties, in particular, zeroth, first and second order moments with high precision. The flexibility of choosing the degree of Bernstein polynomials makes this technique more appropriate for solving such problems to obtain high accuracy. In contrast, the accuracy of Picard's method is strongly dependent of the number of series terms considered and to increase the accuracy, a large number of series terms is required, making it computationally very expensive.

6. Final conclusions, remarks and future prospects

A collocation method based on multistage Bernstein polynomial is developed to solve a very complex nonlinear integro-partial differential equation that arises in a model of the enzymatic coagulation of milk. The accuracy of the proposed method was assessed by evaluating the residual error norm with several different types of kernels. At each sub-interval of the time domain, we apply a newly developed spline-based multistage Bernstein collocation method for the semi-analytic solution. The proposed method is very efficient to solve such a nonlinear complex model in comparison to Picard's method, and equally efficient to more complex discretisation based FVS. Picard's method has also shown its usefulness because it provides an exact solution in case of linear differential equation. But it

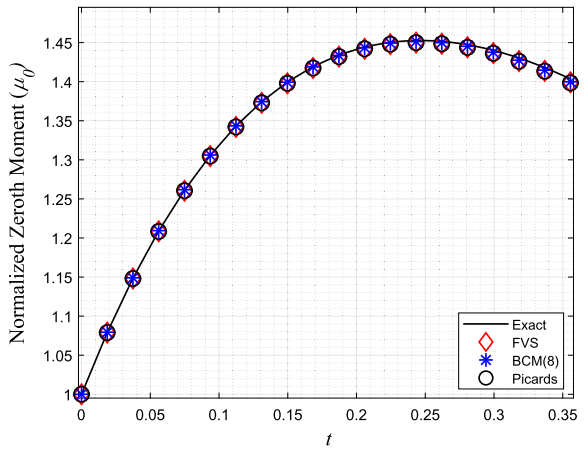

(a) μ_0 at $N = 8$ for $K_1 = 5$

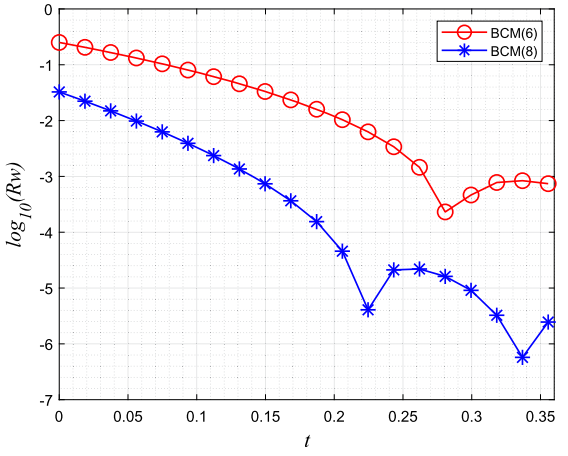

(b) $log_{10}(Rw)$ of μ_0 at $N = 6$ and 8 for $K_1 = 5$

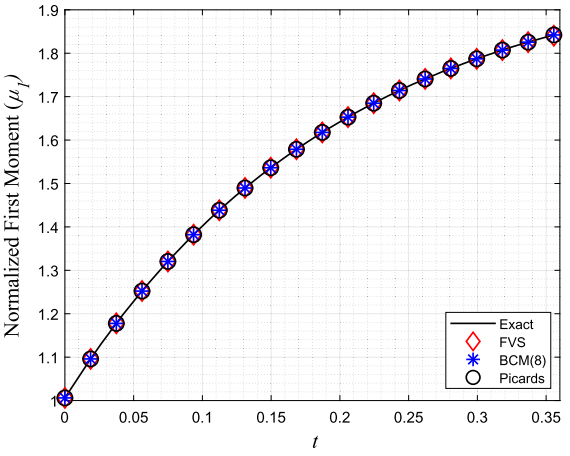

(c) μ_1 at $N = 8$ for $K_1 = 5$

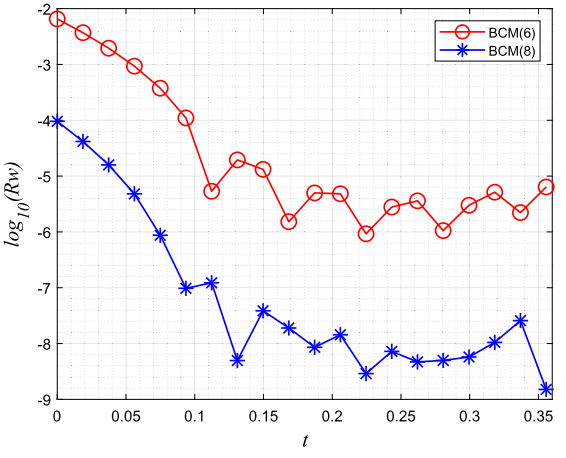

(d) $log_{10}(Rw)$ of μ_1 at $N = 6$ and 8 for $K_1 = 5$

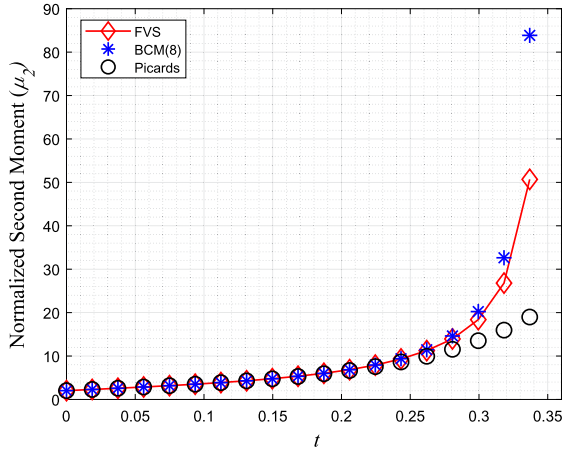

(e) μ_2 at $N = 8$ for $K_1 = 5$

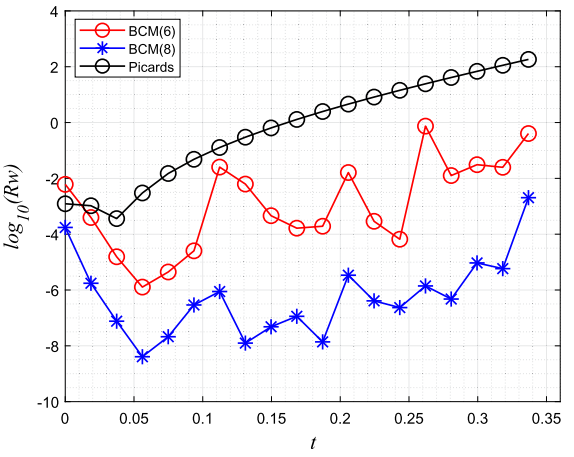

(f) $log_{10}(Rw)$ of μ_2 at $N = 6$ and 8 for $K_1 = 5$

Fig. 7. Testing of different moments for product kernel $\beta(x, y) = xy$ for $K_1 = 5$.

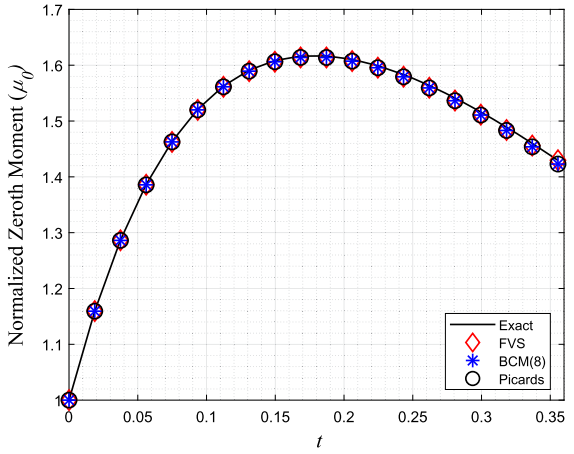

(a) μ_0 at $N = 8$ for $K_1 = 10$

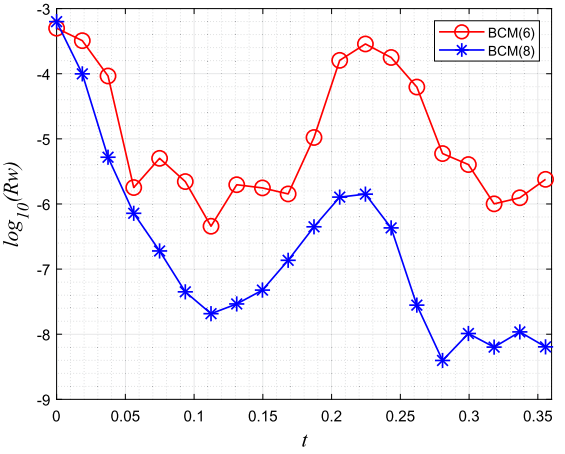

(b) $log_{10}(Rw)$ of μ_0 at $N = 6$ and 8 for $K_1 = 10$

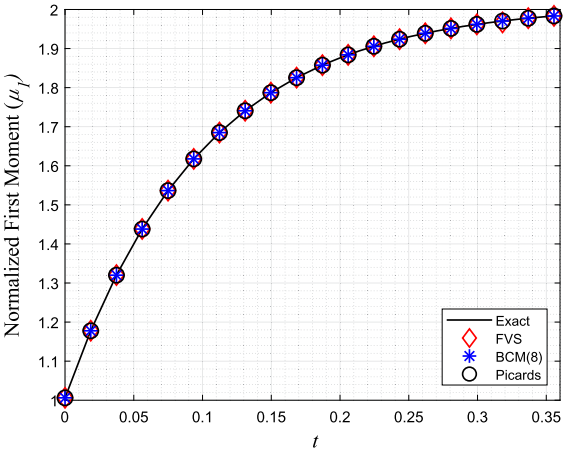

(c) μ_1 at $N = 8$ for $K_1 = 10$

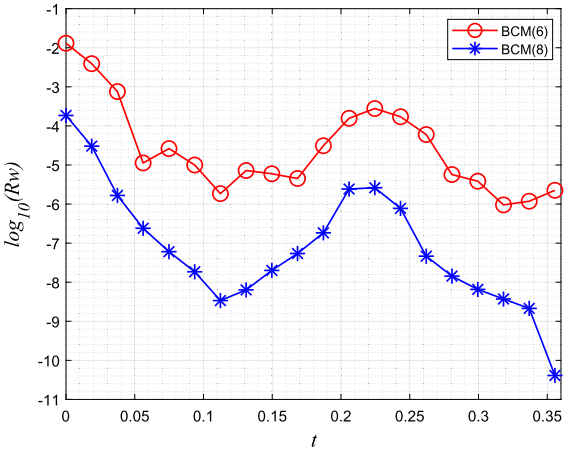

(d) $log_{10}(Rw)$ of μ_1 at $N = 6$ and 8 for $K_1 = 10$

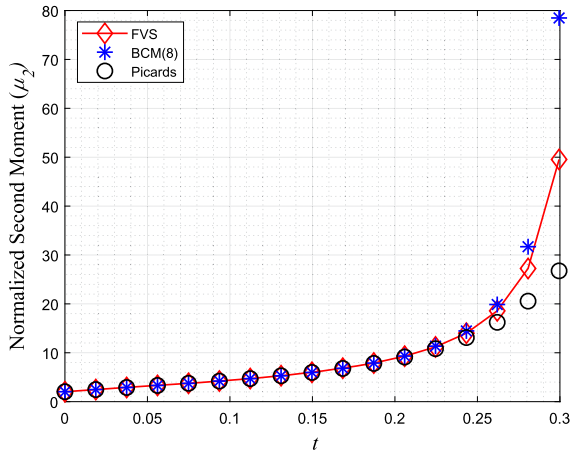

(e) μ_2 at $N = 8$ for $K_1 = 10$

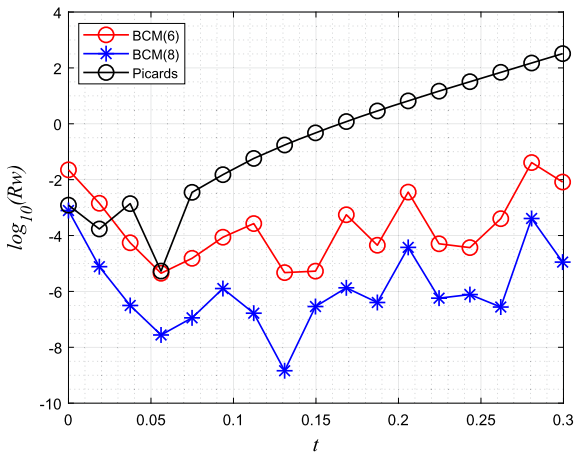

(f) $log_{10}(Rw)$ of μ_2 at $N = 6$ and 8 for $K_1 = 10$

Fig. 8. Testing of different moments for product kernel $\beta(x, y) = xy$ for $K_1 = 10$.

Table 6
Error analysis of the moments for product kernel.

	$K_1 = 5$				$K_1 = 10$			
	Avg_{Rw}		End_{Rw}		Avg_{Rw}		End_{Rw}	
$\mu_p(t)$	BCM(6)	BCM(8)	BCM(6)	BCM(8)	BCM(6)	BCM(8)	BCM(6)	BCM(8)
$\mu_0(t)$	0.057130	0.004744	7.4E-04	2.4E-06	8.2E-05	2.3E-06	3.7E-05	6.3E-09
$\mu_1(t)$	0.000684	7.9E-06	6.3E-06	1.5E-09	9.2E-04	2.2E-06	1.1E-05	4.1E-11
$\mu_2(t)$	0.066937	0.000117	0.403881	0.002032	0.004601	0.008227	7.3E-05	1.1E-05

is not useful for nonlinear differential equations because space and time complexity increase. In such cases, spline-based multi-stage Bernstein collocation method has shown its supremacy. The tables and figures illustrate that the proposed method converges, that is, if we increase the degree of polynomials, accuracy increases. The zero vector was used as the initial guess for all the cases and sub-intervals when evaluating the nonlinear algebraic systems. However, if the problem is stiff and sensitive to the initial guess, finding an appropriate initial guess may require significant effort.

In future, multiple properties of the system will be tracked by solving multidimensional enzymatic coagulation models for cheese coagulation.

CRediT authorship contribution statement

Nikhil Sriwastav: Writing – review & editing, Writing – original draft, Validation, Methodology, Investigation, Formal analysis, Conceptualization. **Ashok Das:** Writing – review & editing, Writing – original draft, Validation, Methodology, Investigation, Formal analysis. **Orest Shardt:** Writing – review & editing, Writing – original draft, Validation, Supervision, Methodology, Formal analysis. **Jitendra Kumar:** Writing – review & editing, Visualization, Validation, Formal analysis. **Mehakpreet Singh:** Writing – review & editing, Writing – original draft, Visualization, Validation, Supervision, Methodology, Investigation, Formal analysis, Conceptualization.

Declaration of competing interest

The authors declare that they have no known competing financial interests or personal relationships that could have appeared to influence the work reported in this paper.

Acknowledgement

This work has been supported by the Dairy Processing Technology Centre funded through Enterprise Ireland, Grant Agreement number: TC 2020 0028.

Appendix A. Methodology-II (Picard's iteration method)

This section introduces a numerical scheme based on Picard's iteration method for the approximate solution of equation (3) to approximate the enzymatic coagulation. The moment equation combines the first two phases of the enzymatic coagulation process, is used to determine the numerical solution to (1). The first order moment has exact solution $\mu_1(t) = M_1(1 - \exp^{-K_1 t}) + \mu_1(0)$, subject to the initial condition $\mu_1(0)$ for every kernel β. The moment equation (3) can be rewritten into the following generalized differential equation

$$\frac{d\mu_p(t)}{dt} = M_p K_1 \exp(-K_1 t) + F(t, \mu_p(t)), \quad t \in [0, T) \text{ and } p = 0, 2, \tag{A.1}$$

for the constant kernel, sum kernel, and the product kernel.

Integrating equation (A.1) from 0 to t over $[0, T)$, we have

$$\mu_p(t) = \mu_k(0) + M_p\left(1 - \exp(-K_1 t)\right) + \int_0^t F(s, \mu_p(s))ds. \tag{A.2}$$

In contrast to Theorem 4.2, there exists a Picard's iterative formula given by

$$\mu_p(t)|_n = M_p(0) + M_p\left(1 - \exp(-k_1 t)\right) + \int_0^t F(s, \mu_p(s)|_{n-1})ds, \text{ for } n \geq 1. \tag{A.3}$$

Here $\mu_p(t)|_n$ is the n^{th} iteration of the approximate solution of $\mu_p(t)$.

Appendix B. Validation of the proposed methodology

To validate the authentication of the proposed methodology, the coefficients of the Bernstein polynomials are tabulated here for $N = 6$ on the sum kernel for proteolytic constant $K_1 = 5$

$\mu_p(t)$	Domain	c_0	c_1	c_2	c_3	c_4	c_5	c_6
$\mu_0(t)$	$t \in [0,1]$	0.990000000	1.616200320	1.160100062	0.908212080	0.673010384	0.508011764	0.384658506
$\mu_0(t)$	$t \in [1,2]$	0.384658506	0.261305248	0.182064098	0.130532372	0.095064400	0.070322364	0.052654326
$\mu_1(t)$	$t \in [0,1]$	1.008800000	1.790909632	1.874814479	1.949736234	1.968671071	1.980901511	1.986565878
$\mu_1(t)$	$t \in [1,2]$	1.986565878	1.992230245	1.992586505	1.993179962	1.993279720	1.993367385	1.993405551
$\mu_2(t)$	$t \in [0,1]$	2.044600000	1.129329156	5.751506264	5.900897593	15.51260925	25.69200763	77.95256668
$\mu_2(t)$	$t \in [1,2]$	77.95256668	624.4970770	2115.257346	3864.665800	4066.856051	2330.910741	585.2217362

Data availability

No data was used for the research described in the article.

References

[1] T. Hagi, A. Kurahashi, Y. Oguro, K. Kodaira, M. Kobayashi, S. Hayashida, H. Yamashita, Y. Arakawa, T. Miura, K. Sato, S. Tomito, S. Sujuki, K.I. Kusumoto, N. Moriya, M. Nomura, Effect of sake lees on cheese components in cheese ripened by aspergillus oryzae and lactic acid bacteria, J. Dairy Sci. 105 (6) (2022) 4868–4881.
[2] M. Britten, H.J. Giroux, Rennet coagulation of heated milk: a review, Int. Dairy J. 124 (2022) 105179.
[3] D.B. Hyslop, Enzyme-induced coagulation of casein micelles: a number of different kinetic models, J. Dairy Res. 60 (4) (1993) 517–533.
[4] D. Ramkrishna, Theory and Applications to Particulate Systems in Engineering. Population Balances, Academic Press, San Diego, 2000.
[5] N.I. Kolev, Multiphase Flow Dynamics 1- Fundamentals, Springer-Verlag GmbH, Berlin, Germany, 2002.
[6] A. Borissova, G. Goltz, J.P. Kavanagh, T. Wilkins, Reverse engineering the kidney: modelling calcium oxalate monohydrate crystallization in the nephron, Med. Biol. Eng. Comput. 48 (2010) 649–659.
[7] H. Amini, X. He, Y.C. Tseng, G. Kucuk, R. Schwabe, L. Schultz, M. Maus, D. Schröder, P. Rajniak, E. Bilgili, A semi-theoretical model for simulating the temporal evolution of moisture-temperature during industrial fluidized bed granulation, Eur. J. Pharm. Biopharm. 151 (2020) 137–152.
[8] H. Zhao, C. Zheng, A stochastic simulation for the collection process of fly ashes in single-stage electrostatic precipitators, Fuel 87 (10–11) (2008) 2082–2089.
[9] E. Sherer, R.E. Hannemann, A. Rundell, D. Ramkrishna, Estimation of likely cancer cure using first- and second-order product densities of population balance models, Ann. Biomed. Eng. 35 (2007) 903–915.
[10] A. McBride, A.L. Smith, W. Lamb, Strongly differentiable solutions of the discrete coagulation–fragmentation equation, Phys. D, Nonlinear Phenom. 239 (15) (2010) 1436–1445.
[11] B. Niethammer, J.J.L. Velazquez, Self-similar solutions with fat tails for Smoluchowski's coagulation equation with locally bounded kernels, Commun. Math. Phys. 318 (2) (2013) 505–532.
[12] F. Rezakhanlou, Moment bounds for the solutions of the Smoluchowski equation with coagulation and fragmentation, Proc. R. Soc. Edinb., Sect. A, Math. 140 (5) (2010) 1041–1059.
[13] Z.A. Melzak, A scalar transport equation, Trans. Am. Math. Soc. 85 (2) (1957) 547–560.
[14] W.T. Scott, Analytic studies of cloud droplet coalescence I, J. Atmos. Sci. 25 (1) (1968) 54–65.
[15] P.B. Dubovskii, V.A. Galkin, I.W. Stewart, Exact solutions for the coagulation-fragmentation equation, J. Phys. A, Math. Gen. 25 (18) (1992) 4737.
[16] G. Kaur, R. Singh, M. Singh, J. Kumar, T. Matsoukas, Analytical approach for solving population balances: a homotopy perturbation method, J. Phys. A, Math. Theor. 52 (38) (2019) 385201.
[17] T. De, A. Das, M. Singh, J. Kumar, Enhancing efficiency in particle aggregation simulations: coarse-grained particle modeling in the dem-pbm coupled framework, Comput. Methods Appl. Mech. Eng. 417 (2023) 116436.
[18] A. Majumder, V. Kariwala, S. Ansumali, A. Rajendran, Lattice Boltzmann method for population balance equations with simultaneous growth, nucleation, aggregation and breakage, Chem. Eng. Sci. 69 (1) (2012) 316–328.
[19] F. Filbet, P. Laurençot, Numerical simulation of the Smoluchowski coagulation equation, SIAM J. Sci. Comput. 25 (6) (2004) 2004–2028.
[20] M. Singh, H.Y. Ismail, T. Matsoukas, A.B. Albadarin, G. Walker, Mass-based finite volume scheme for aggregation, growth and nucleation population balance equation, Proc. R. Soc. A 475 (2231) (2021) 20190552.
[21] M. Singh, New finite volume approach for multidimensional Smoluchowski equation on nonuniform grids, Stud. Appl. Math. 147 (3) (2021) 955–977.
[22] J. Kumar, G. Warnecke, Convergence analysis of sectional methods for solving breakage population balance equations-I: the fixed pivot technique, Numer. Math. 111 (1) (2008) 81–108.
[23] J. Kumar, G. Warnecke, Convergence analysis of sectional methods for solving breakage population balance equations-II: the cell average technique, Numer. Math. 110 (4) (2008) 539–559.
[24] P. Kushwah, A. Paswan, V. Thota, J. Saha, M. Singh, K. Moroney, New semi-analytical approach and its convergence analysis for a classical hyperbolic fragmentation model: a homotopy perturbation method, J. Comput. Sci. 73 (2023) 102135.
[25] S. Yadav, A. Das, S. Singh, S. Tomar, R. Singh, M. Singh, Coupled approach and its convergence analysis for aggregation and breakage models: study of extended temporal behaviour, Powder Technol. 439 (2024) 119714.
[26] M. Singh, S. Shirazian, V. Ranade, G.M. Walker, A. Kumar, Challenges and opportunities in modelling wet granulation in pharmaceutical industry–a critical review, Powder Technol. (2022) 117380.
[27] M. Singh, V. Ranade, O. Shardt, T. Matsoukas, Challenges and opportunities concerning numerical solutions for population balances: a critical review, J. Phys. A, Math. Theor. 55 (38) (2022) 383002.
[28] S.B. Lomholt, P. Worning, L. Øgendal, K.B. Qvist, D.B. Hyslop, R. Bauer, Kinetics of the renneting reaction followed by measurement of turbidity as a function of wavelength, J. Dairy Res. 65 (4) (1998) 545–554.
[29] D.B. Hyslop, Enzymatically initiated coagulation of casein micelles: a kinetic model, Neth. Milk Dairy J. 43 (1989) 163–170.
[30] J. Rashidinia, A. Tahmasebi, Approximate solution of linear integro-differential equations by using modified Taylor expansion method, World J. Model. Simul. 9 (4) (2013) 289–301.

[31] P. Pathak, A.K. Barnwal, N. Sriwastav, R. Singh, M. Singh, An algorithm based on homotopy perturbation theory and its mathematical analysis for singular nonlinear system of boundary value problems, Math. Methods Appl. Sci. (2023) 1–22, https://doi.org/10.1002/mma.9299.
[32] A. Shannon, F. Dubeau, M. Uysal, E. Özkan, A difference equation model of infectious disease, Int. J. Bioautom. 26 (4) (2022).
[33] R. Singh, J. Kumar, The Adomian decomposition method with Green's function for solving nonlinear singular boundary value problems, J. Appl. Math. Comput. (2014) 397–416.
[34] M. Marin, A. Öchsner, M.M. Bhatti, Some results in Moore-Gibson-Thompson thermoelasticity of dipolar bodies, Z. Angew. Math. Mech. 100 (12) (2020) 202000090.
[35] S. Vlase, M. Marin, M.L. Scutaru, R. Munteanu, Coupled transverse and torsional vibrations in a mechanical system with two identical beams, AIP Adv. 7 (6) (2017).
[36] F.I. Haq, S.U. Islam, I.A. Tirmizi, A numerical technique for solution of the MRLW equation using quartic B-splines, Appl. Math. Model. 34 (12) (2010) 4151–4160.
[37] A. Iqbal, N.N.A. Hamid, A.I.M. Ismail, Cubic B-spline Galerkin method for numerical solution of the coupled nonlinear Schrödinger equation, Math. Comput. Simul. 174 (2020) 32–44.
[38] A. Iqbal, N.N.A. Hamid, A.I.M. Ismail, Soliton solution of Schrödinger equation using cubic B-spline Galerkin method, Fluids 4 (2) (2019) 108.
[39] N. Sriwastav, A.K. Barnwal, A.M. Wazwaz, M. Singh, A novel numerical approach and stability analysis for a class of pantograph delay differential equation, J. Comput. Sci. 67 (2023) 101976.
[40] S. Albosaily, Y. Quintana, A. Iqbal, W.A. Khan, Lagrange-based hypergeometric Bernoulli polynomials, Symmetry 14 (6) (2022) 1125.
[41] N. Sriwastav, A.K. Barnwal, H. Ramos, R.P. Agarwal, M. Singh, Advanced numerical scheme and its convergence analysis for a class of two-point singular boundary value problems, Math. Comput. Simul. 216 (2024) 30–48.
[42] N. Saha, R. Singh, Numerical and mathematical analysis of nonlocal singular Emden–Fowler type bvps by improved Taylor-wavelet method, Comput. Appl. Math. 43 (5) (2024) 280.
[43] D. Guo, V. Lakshmikantham, Nonlinear Problems in Abstract Cones, vol. 5, Academic Press, San Diego, USA, 2014.
[44] L. Forestier-Coste, S. Mancini, A finite volume preserving scheme on nonuniform meshes and for multidimensional coalescence, SIAM J. Sci. Comput. 34 (6) (2012) B840–B860.
[45] M. Singh, N. Sriwastav, O. Shardt, Efficient mass-preserving finite volume approach for the rennet-induced coagulation equation, Chaos Solitons Fractals 181 (2024) 114692.